



## Use of voxelized thyroid models to develop a physical-anthropomorphic phantom for 3D printing

Moratelli<sup>a</sup> T. S., Soares<sup>a</sup> A. B., Lucena<sup>a</sup> E. A., Dantas<sup>a</sup> A. L. A., Mendes<sup>b</sup> B. M., Félix<sup>c</sup>  
P. S. S., Bourguignon<sup>c</sup> F. L., Dórea<sup>c</sup> M. M., Romani<sup>c</sup> E. C., Dantas<sup>a</sup> B. M.

<sup>a</sup>*Institute of Radioprotection and Dosimetry, 22783-116, Salvador Allende Avenue s/n, Rio de Janeiro – RJ - Brazil.*

<sup>b</sup>*CNEN Nuclear Technology Development Center, Radiation Dosimetry Section - SECDOS.*

*Presidente Antônio Carlos Avenue, 6.627, Campus da UFMG – Pampulha – MG - Brasil*

<sup>c</sup>*FIRJANSENAI, 20911-210, Praça Natividade Saldanha, 19 - Rio de Janeiro – RJ - Brasil*

*tayrine.moratelli@gmail.com*

---

### ABSTRACT

The monitoring of the intake of radionuclides by workers and members of the public using in vivo measurements requires the application of calibration factors obtained with physical-anthropomorphic phantoms. In the case of <sup>131</sup>I, the lack of anatomical realism of the phantom might impair the quality and reliability of the monitoring result. Thus, in order to develop a realistic physical thyroid phantom using 3D printing, images of the voxelized models provided in ICRP 110 were used. The superposition of the images of the original model and the treated model demonstrate the maintenance of morphological characteristics. Therefore, image manipulation techniques applied in this work aimed to smooth the sharp angles of the original image and the prototype printing were considered effective.

**Keywords:** Thyroid-neck simulator; Voxelized models; <sup>131</sup>I; 3D printing.

---



## 1. INTRODUCTION

Individual monitoring is one of the radiological protection tools to assess effective dose or equivalent doses received by an occupationally exposed individual (OEI) from any type of external or internal exposure. All workers with a potential risk of exposure to annual doses exceeding the registry level of 1 mSv per year must undergo an individual monitoring program that must be included in the radiological protection program of the facility [1].

In nuclear medicine the routine handling of  $^{131}\text{I}$  unsealed sources results in a significant risk of intake through inhalation and ingestion and, consequently, internal exposure. This risk is associated to the fact that iodine is a volatile element at room temperature. In addition,  $^{131}\text{I}$  isotope has the highest internal dose coefficient among the radionuclides used for diagnosis [2-4].

The biokinetic model for  $^{131}\text{I}$  is described in ICRP 67 [5], where it is admitted that upon transfer to the blood, about 30% of  $^{131}\text{I}$  activity is retained in the thyroid gland, while about 70% is excreted directly in urine. The biological half-life in the blood is about 0.25 days (~ 6 hours), in the thyroid gland about 80 days, and in other tissues 12 days on average. It is known that a large part of the radionuclide (80%) returns to the blood circulation and will be absorbed by the thyroid gland and excreted in urine; the rest (20%) is excreted in feces [6].

Internal monitoring of  $^{131}\text{I}$ , which decays by emission of  $\beta$ -particles and gamma radiation, can be performed through *in vivo* measurements [7]. Quantification of the activity retained in the body using this technique requires the application of calibration factors obtained with physical-anthropomorphic phantom of the organs and tissues of interest. Such factors allow converting the count rate recorded in the measurement into activity in the organ. In some cases, the approximate shape of these phantoms are sufficient to obtain reliable calibration factors [8], but in other situations, as in the case of  $^{131}\text{I}$ , the lack of anatomical realism may impair the quality and reliability of the monitoring result [9-11].

New 3D printing technologies have shown to be economically viable alternatives for producing physical-anthropomorphic phantoms for use in medical applications. Obtaining structures with realistic level of detail, printed from three-dimensional real human images, using artificial or natural tissue-equivalent materials with physicochemical properties similar to the living tissues that they are intended to simulate, become a reality in recent years [12-16]. These new, more realistic 3D-

printed models can contribute to the reduction of errors in estimates of radionuclide intakes in routine monitoring and in the evaluation of accidents involving  $^{131}\text{I}$  intake.

Due to the lack of training of Radiation Protection Officers in bioassay techniques and the costs and logistics associated to the implementation of routine internal monitoring programs in nuclear medicine services, this requirement has not been fulfilled on a regular basis. However, the improvement of physical models allows performing internal monitoring at the workplace using equipment available in the clinic itself, such as gamma cameras, uptake probes and surface contamination monitors, as a feasible alternative [17,18].

Based on medical imaging of patients and data provided in ICRP Publication 89 [19] on the reference anatomical and physiological parameters for men and women, ICRP 110 [20] describes the development and application of computer anthropomorphic phantoms of reference adults. Essentially, the two voxelized models provided, RCP\_AM (male) and RCP\_AF (female), are composed by two-dimensional images that, when superimposed, set up three-dimensional images that can be 3D printed. Such phantoms have been segmented into more than 130 different organs and tissues including the thyroid. The RCP\_AF model can be seen in Figure 1A. The thyroid was highlighted in red. Magnified rendered images of the thyroid are shown in Figures 1B and 1C.

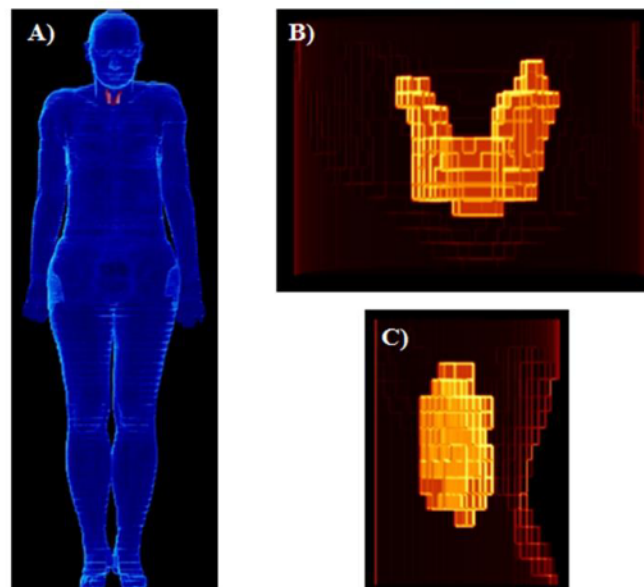


**Figure 1:** Female voxelized computational phantom of the ICRP. A) Rendering of the phantom highlighting the thyroid in red. B) Magnified front view of the phantom in the thyroid region. C) Magnified side view of the phantom in the thyroid region.

The present study aimed to develop a specific thyroid model, based on the images of the RCP\_AF reference voxelized model provided by ICRP 110 [20]. Such model, sufficiently realistic, is used to obtain a physical-anthropomorphic thyroid phantom, printed using 3D technology.

## 2. MATERIALS AND METHODS

### 2.1. Obtaining a realistic 3D image of the thyroid

In this phase, a high-resolution, anatomically representative computational model of the thyroid is obtained. Voxelized models from ICRP 110 [20] provide the segmented thyroid. In this work we used the female model (RCP\_AF), presented in Figure 1A. This choice was due to its higher resolution ( $1.775 \times 1.775 \times 4.84 \text{ mm}^3$ ) compared to the male model ( $2.137 \times 2.137 \times 8.0 \text{ mm}^3$ ) [20].

The flowchart for obtaining the detailed thyroid model is shown in Figure 2. ImageJ® software [21] was used to shape and manage the operations with the images.

First step was the setup of the relevant region, avoiding working with a large number of images without significant information (Step 1 - Figure 2). The RCP\_AF model is composed of 299 images in the XY plane, stacked on the Z axis. The RAW format image of the RCP\_AF phantom was loaded into ImageJ and saved as a sequence of TIF format images in the XY plane. The image slices numbered as 036 to 070, referring to the region of the model that contains the thyroid, were kept and the others deleted.

Although the resolution of the female model is higher than the reference male model, the level of detail of the thyroid was considered lower than desirable for a specific model of this organ, as can be seen in Figures 1B and 1C. Therefore, in the next step the resolution of the model was increased (Step 2 - Figure 2). The ImageJ command "Image → Scale" was used to reduce the size of the voxels while maintaining the size of the images. The factor 3.55 was used for the X and Y axis and the factor 9.68 for the Z axis. The image matrix was changed from (301 x 139 x 35) to (1068 x 493 x 338) and the voxel dimensions were changed to ( $0.5 \times 0.5 \times 0.5 \text{ mm}^3$ ). No interpolation was used at this stage.

The "VoxelPhantoms Tools" command, developed specifically for ImageJ, was used to generate two distinct models from the image of the relevant region of the RCP\_AF: a model of the thyroid

and a model in which all tissues were converted to "soft\_tissue". Subsequently, the command "Process → Binary → Makebinary" was applied to both models (Steps 3a and 3b - Figure 2). This process converts the pixel value to 0 or 255. A threshold is set. If the voxel value is higher than the threshold, the voxel value is converted to 255. If it is lower, it becomes 0. In practice, for 8-bit images, the pixels become black or white by eliminating grayscale.

A 3D Gaussian blur was applied to the binary images of the models in order to smooth the sharp angles originated from the large voxel dimensions of the original model (Steps 4a and 4b - Figure 2). The ImageJ command "Process → Filters → GaussianBlur" was used. A sigmoidal radius of 5.0 was adopted.

Voxels with different shades of gray are generated in the models by the blurring procedure. The "Image → Adjust → Threshold" command was used to reconvert the models into binary images (Steps 5a and 5b - Figure 2). The threshold value was determined by trial and error so that the resulting model had the closest possible volume to the original model. The thyroid of the RCP\_AF model, highlighted in red in Figure 2A, has a volume of 16.4 cm<sup>3</sup> and a mass of 17g [20].

The two models were then merged into a single model with two segmented tissues: thyroid and soft tissue (Step 6 - Figure 2). Before merging, the "Voxel Phantoms Tools" command was used to change the value of the voxels of the two models. The voxels with a value of 255 were changed to 100 in the soft tissue model. In the thyroid model, the value was changed from 255 to 150. The models were then merged using the command "Process → Image Calculator" of ImageJ. The soft tissue model image was added to the thyroid model image. The resulting three-dimensional image had the soft tissue voxels segmented with the 100 code and the thyroid with 250 code.

In the last step, the model was reduced to the size required for 3D printing (Step 7 - Figure 2). For this purpose, a circular mask of 220 pixels (11.0 cm) diameter was positioned to delimit the neck region, so that the thyroid was positioned in the center of the semicircle. The command "Edit → ClearOutside" was used, followed by the command "Image → Crop".

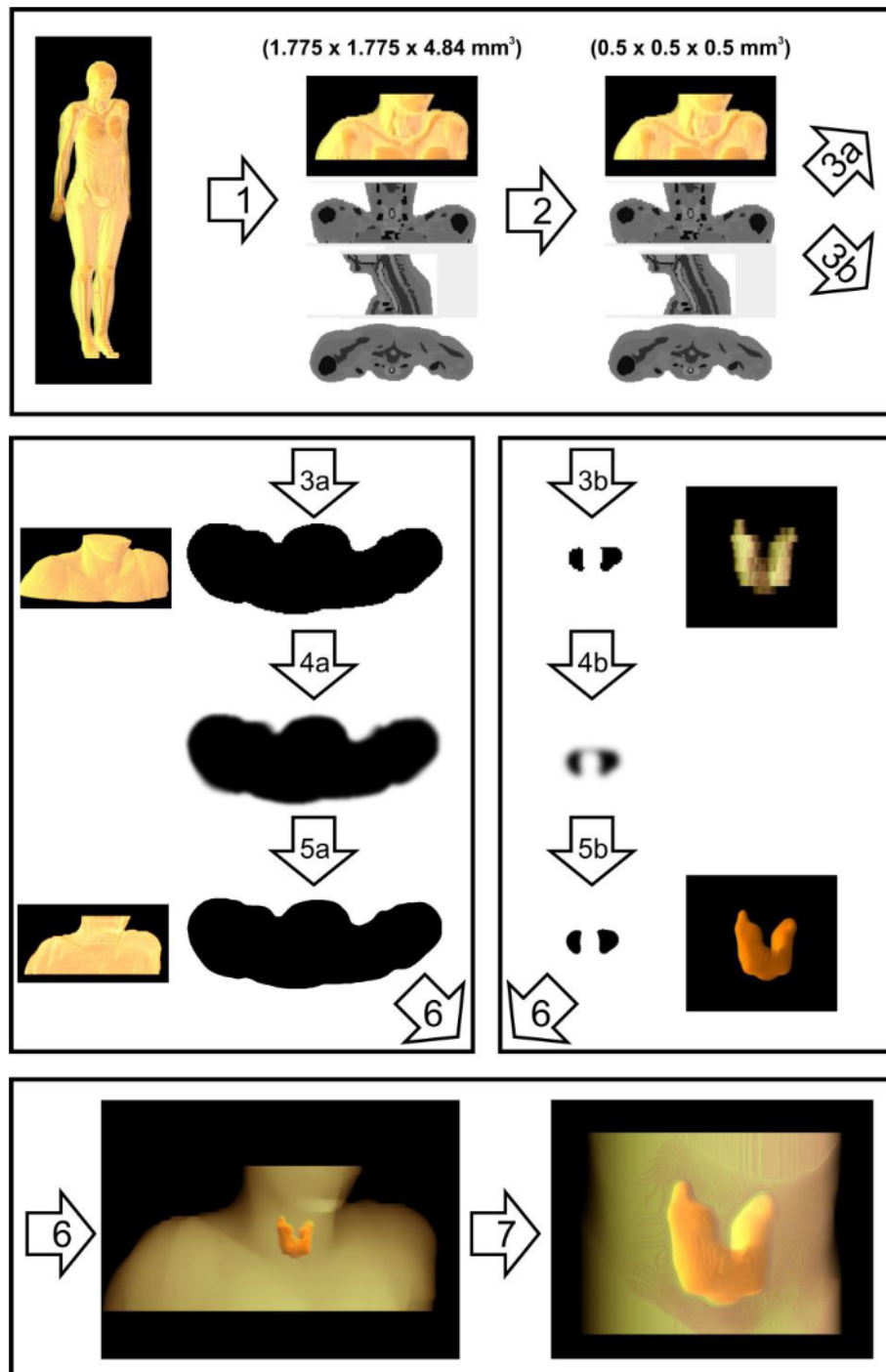


**Figure 2:** Flowchart of the process of obtaining the detailed thyroid model. 1) Selection of the relevant region. 2) Increasing the resolution of the model. 3a) and 3b) Binarization of the images and obtaining two models (soft tissue and thyroid). 4a and 4b) Gaussian blurring to smooth the angles. 5a) and 5b) Re-binning of the smoothed models. 6) Fusion of the thyroid and soft tissue models. 7) Cutting for model reduction.

Finally, the resulting thyroid volume was measured and compared to the original volume. The Amide<sup>®</sup> software was used to measure the length of the lobes for comparison with literature data. In addition, the original model image and the high-resolution model were superimposed to check if the thyroid and neck anatomy did not change significantly after the manipulation procedures of the original image.

## 2.2. 3D printed thyroid model

After image manipulation, voxelized model was converted into a three-dimensional model in ".STL" format. The STL file is widely used because it is simple, light, and easy to handle by 3D software and printers. These files were treated in the 3DsMax software for the model parts improvement.

3DsMax is the most used program by modeling teams and can be applied in several segments of 3D models development. The 3DsMax software is a tool usually applied to the manipulation of three-dimensional elements, with 3D mesh modifiers, which facilitated the construction and editing of shapes needed for research, as well as accepting the import and export of several file formats, including those compatible with slicing software for 3D printing (Figure 3 and Figure 4).

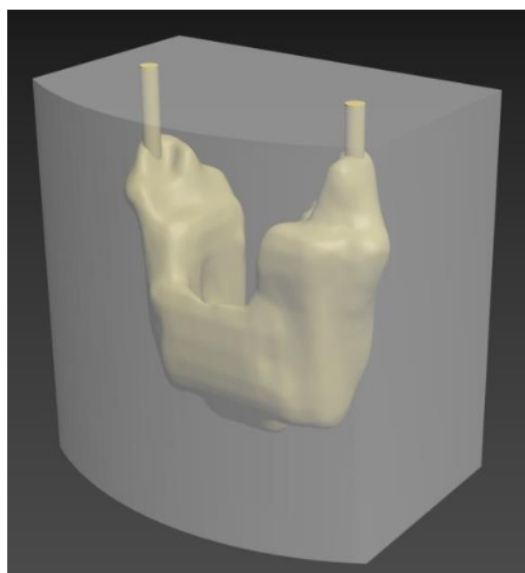


**Figure 3:** 3D model of the Thyroid Phantom, for visualization of thyroid volume.

In simple terms, the STL file format uses a series of linked triangles to recreate the surface geometry of a solid model. For a basic model, its surfaces can be represented using a few triangles. For higher resolution models, more triangles are needed to replicate the model surface. The more triangles that make up a model, the larger the file size and the more detailed the object.

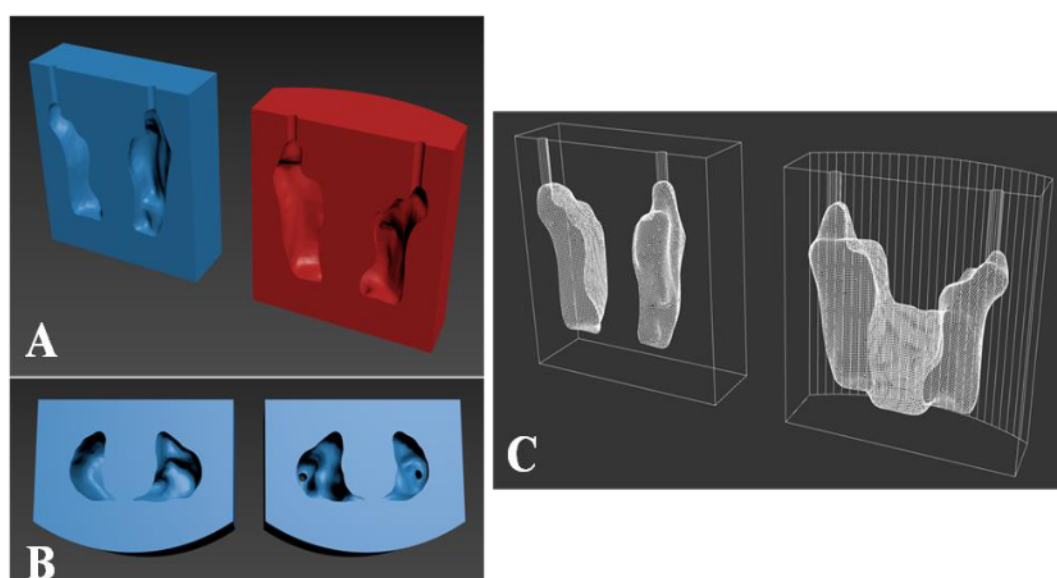


**Figure 4:** 3D models of the Thyroid Phantom: (a) vertical cut, referring to the posterior (blue) and frontal (red) portions; (b) horizontal cut, referring to the upper (right side) and lower (left side) portions; (c) wireframe image of the vertical models, referring to the posterior (left side) and frontal (right side) portions.

For 3D printing, the Ultimaker CURA software was used to slice and visualize the thyroid model before printing the phantom (Figure 5). Parameters as anatomical detailing of the thyroid, height, width, volume and distance between the volume that characterizes the thyroid and the wall that simulates the anterior portion of the neck were checked according to the RCP\_AF ICRP 110 model [20].

Preliminary print settings include, among other parameters, the table temperature, extrusion temperature, amount of inner and outer wall, layer thickness, type and percentage of part fill, print



speed, amount of base and top layer.

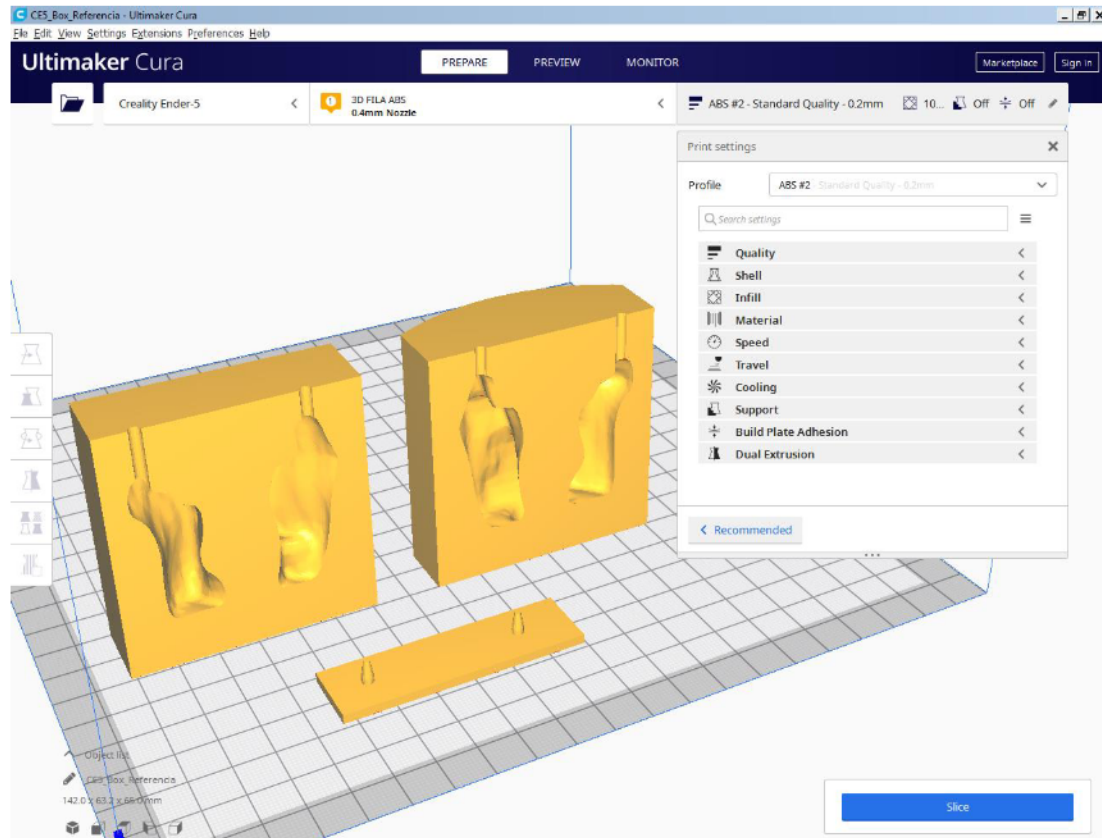


**Figure 5:** *Ultimaker Cura software screen.*

### 3. RESULTS AND DISCUSSION

#### 3.1. Realistic 3D Thyroid Model

The high-resolution thyroid computational model obtained based on the female phantom of ICRP 110 [20] is shown in Figure 6. It can be seen that the image manipulation techniques were effective in smoothing out the sharp angles originating from the relative low resolution of the original image without, however, significantly altering the size and the shape of the organ. The volume obtained for the thyroid in this model was 16.44 cm<sup>3</sup>, i.e., 0.3% larger than the reference.

The morphology of the resulting model kept good anatomical representation with the characteristic butterfly shape [22]. The lobes (left and right) connected by the region called the isthmus also can be visualized. The left lobe presented a length of 4.0 cm and the right lobe 4.6 cm. According to Maciel [23], the length of the lobes in normal individuals varies from 3 to 5 cm.

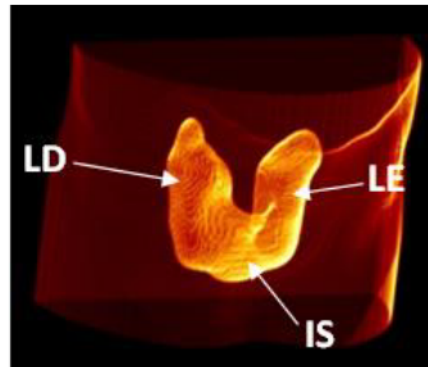


**Figure 6:** Tilted view of the 3D rendering of the high-resolution anthropomorphic thyroid computer model with right (*LD*) and left (*LE*) lobes connected by the isthmus (*IS*).

Figure 7 shows the superposition of the images of the original model and the high-resolution model. These juxtaposed images demonstrate the maintenance of morphological characteristics important for its use in internal dosimetry such as the size and position of the thyroid in the neck and its distance from the skin.

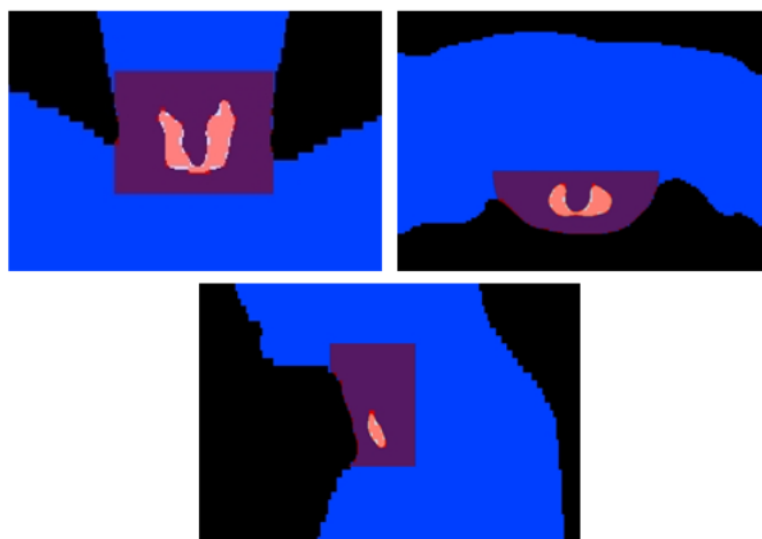


**Figure 7:** *Superposition of the original RCP\_AF model and the high-resolution thyroid model.*

### 3.2. Printed Thyroid Template

The prototypes of the physical-anthropomorphic thyroid phantom obtained based on the female model from ICRP 110 [20] are shown in Figure 8. These fabricated prototypes clearly show the lines and contour of the walls for the feasibility of using 3D printing to produce the phantom. The technique has a limitation of building a totally empty internal space, having the need for connecting supports that are inserted inside the empty space, but some tests are promising as we can notice in the one-piece printing. Thus, at the first moment, it was decided to make a cut in two parts of the mold, which can be seen in the detail of figure 8. Note that the void represents the thyroid volume, where the liquid solution of the radioactive  $^{133}\text{Ba}$  standard ( $^{131}\text{I}$  simulator for gamma spectrometry purposes) will be added. Thus, the final print of the full-scale female phantom can be made, which is subsequently fitted to the polyethylene neck phantom produced in the mechanical workshop of the Institute of Radioprotection and Dosimetry - IRD/CNEN, in order to compose the full neck-thyroid phantom set.

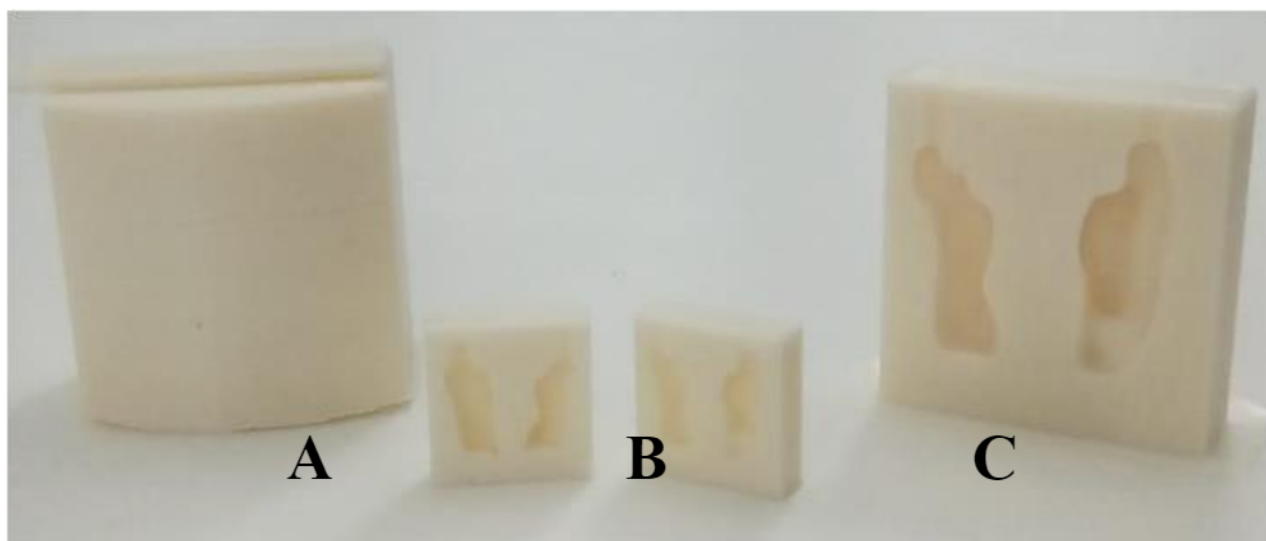


**Figure 8:** *3D printed models of the Thyroid Simulator. Single piece model (A), miniature model (B) and posterior portion - model divided into 2 pieces (C).*

#### 4. CONCLUSION

It can be concluded that the image manipulation techniques employed in this study were effective in smoothing the acute angles originating from the relative low resolution of the original image of the voxelized model. It is also noteworthy that the size of the organ did not change significantly in volume, resulting in only about 0.3% larger than the reference.

Overlapping the images of the original model and the high-resolution model, it can be observed that the morphological characteristics, such as the size and position of the thyroid in the neck and its distance from the skin, were maintained, which is essential for its use in internal dosimetry.

It was observed that the printing techniques were effective since it is possible to state that the organ morphology was maintained, keeping direct relationship with the computational model.

The results obtained in this work allowed the printing of the final phantom with the original dimensions that keep the size, volume and position of the thyroid in the neck. The next phase will be filling the 3D printed phantom with  $^{133}\text{Ba}$  standard solution to perform calibration tests.

#### REFERENCES

- [1] INTERNATIONAL ATOMIC ENERGY AGENCY (IAEA) (2014). Radiation Protection and Safety of Radiation Sources: International Basic Safety Standards. General Safety Requirements Part 3No. GSR Part 3.
- [2] INTERNATIONAL ATOMIC ENERGY AGENCY (IAEA). (1999) Assessment of Occupational Exposure Due to Intakes of Radionuclides - Safety Standards Series, no.RS-G-1.2, IAEA.
- [3] MILLER, K.L.; BOTT, S.M.; VELKLEY, D. E.(1979) "Review of contamination and exposure hazards associated with therapeutic uses of radioiodine". J. Nucl. Med. Technology, v.7, p. 163-166.
- [4] OLIVEIRA, R. S., LEÃO, A. M. A. C. (2008) "History of Radiopharmacy and the implications of Constitutional Amendment N. 49". *Brazilian Journal of Pharmaceutical Sciences*, v. 44, n. 3, p. 377-382.
- [5] ICRP, 1993, Age-dependent Doses to Members of the Public from Intake of Radionuclides -Part 2 Ingestion Dose Coefficients. ICRP Publication 67. Ann. ICRP 23 (3-4).

- [6] ICRP, 1997. Individual Monitoring for Internal Exposure of Workers (preface and glossary missing). ICRP Publication 78. Ann. ICRP 27 (3-4).
- [7] INTERNATIONAL ATOMIC ENERGY AGENCY (IAEA). (1996). Direct methods for measuring radionuclides in the human body. Safety Series n. 114.
- [8] ZHANG, B.; MILLE, M.; XU, X. G.(2008)"An analysis of dependency of counting efficiency on worker anatomy for in vivo measurements: whole-body counting". *Phys. Med. Biol.* 53 3463–75.
- [9] DANTAS, B. M. (1998) "Basis for the calibration of whole-body counters using anthropomorphic physical simulators." PhD Thesis. Universidade do Estado do Rio de Janeiro.
- [10] BROGGIO, D.; ZHANG, B.; DE CARLAN, L.; DESBRÉE, A.; LAMART, S.; LE GUEN, B.; BAILLOEUIL, C.; FRANCK, D. (2009) "Analytical and Monte Carlo assessment of activity and local dose after a wound contamination by activation products". *Health Phys.* 96 155–63.
- [11] LAMART, S.; BLANCHARDON, E.; MOLOKANOV, A.; KRAMER, G. H.; BROGGIO, D.; FRANCK, D. (2009) "Study of the influence of radionuclide biokinetics on the efficiency of in vivo counting using Monte Carlo simulation". *Health Phys.* 96 558–67.
- [12] ZOU, W. et al (2015)"Potential of 3D printing technologies for fabrication of electron bolus and proton compensators". *J. Appl. Clin. Med. Phys.* 16 90–8.
- [13] RUITERS, S.; SUN, Y.; DE JONG, S.; POLITIS, C.; MOMBAERTS, I. (2016) "Computer-aided design and three-dimensional printing in the manufacturing of an ocular prosthesis" *Br. J. Ophthalmol.* 100 879–81.
- [14] ZUNIGA, J. M.; PECK, J.; SRIVASTAVA, R.; KATSAVELIS, D.; CARSON, A. (2016) "An open source 3D-printed transitional hand prosthesis for children". *J. Prosthet. Orthot.* At press (<https://doi.org/10.1097/JPO.000000000000097>).
- [15] TAN, E. T. W.; LING, J. M. AND DINESH, S. K. (2016) "The feasibility of producing patient-specific acrylic cranioplasty implants with a low-cost 3D printer". *J. Neurosurg.* 124 1531–7.
- [16] BEAUMONT, T.; IDEIAS, P. C.; RIMLINGER, M.; BROGGIO, D.; FRANCK, D. (2017) "Development and test of sets of 3D printed age-specific thyroid phantoms for <sup>131</sup>I measurements". *Phys. Med. Biol.* 62 4673.
- [17] LUCENA, E. A.; REBELO, A. M. O.; ARAÚJO, F.; SOUSA, W. O.; DANTAS, A. L. A.; DANTAS, B. M.; CORBO, R. (2007) Evaluation of internal exposure of nuclear medicine staff through in vivo and in vitro bioassay techniques. *Radiation Protection Dosimetry*, v.127, p.465 468.
- [18] OLIVEIRA, S. M.; DANTAS, A. L. A.; DANTAS, B. M. (2016) Comparison of surface contamination monitors for in vivo measurement of <sup>131</sup>I in the thyroid. *Journal of Physics: Conference Series*, Volume 733, Number 1.
- [19] ICRP, 2002, Basic Anatomical and Physiological Data for Use in Radiological Protection Reference Values. ICRP Publication 89. Ann. ICRP 32 (3-4).

- [20] ICRP Publication 110. Adult Reference Computational Phantoms. *Ann ICRP*, v. 39(2), p. 1-166, 2009.
- [21] RASBAND, W.S., (2016) ImageJ, U. S. National Institutes of Health, Bethesda, Maryland, USA. Disponível em: <http://imagej.nih.gov/ij/>. Acessado em Setembro (2016).
- [22] JUNQUEIRA, L. C.; CARNEIRO J. *Basic Histology* 10. ed. São Paulo: Guanabara Koogan, 2004.
- [23] MACIEL, L. M.Z. (2007) The physical examination of the thyroid. *Medicina (Ribeirão Preto)*; 40 (1): 72-77.